Journal of
Materials Chemistry C

Accepted Manuscript

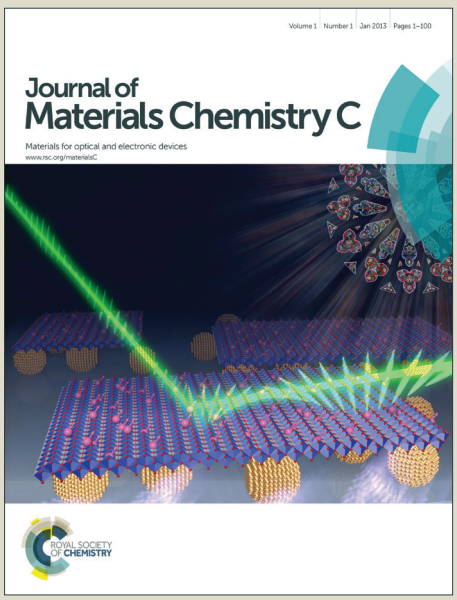

ROYAL SOCIETY OF CHEMISTRY

www.rsc.org/materialsC

Alkoxide-intercalated CoFe-layered double hydroxides as precursors of colloidal nanosheet suspensions: structural, magnetic and electrochemical properties

Gonzalo Abellán,[a] Jose A. Carrasco,[a] Eugenio Coronado,[a,*] Jorge Romero,[a] María Varela,[b,c]

[a] *Instituto de Ciencia Molecular (ICMol), Universidad de Valencia, Catedrático José Beltrán 2, 46980, Paterna, Valencia, Spain.*

[b] *Oak Ridge National Laboratory, Materials Science and Technology Division, Oak Ridge, TN 37830-6071, USA.*

[c] *Universidad Complutense de Madrid, Dpt. Fisica Aplicada III & Instituto Pluridisciplinar. Madrid 28040, Spain.*

* Corresponding author. Tel.: +34 96 354 4415. Fax: +34 96 354 3273. *E-mail address*: eugenio.coronado@uv.es

Abstract

Alkoxide-intercalated CoFe-layered double hydroxides (CoFe-LDHs) were synthesized *via* non-aqueous methanolic route. According with powder X-ray diffraction and field emission scanning electron microscopy, they exhibit a nanosized plate-like morphology with a basal space of 9.21 Å. The hydrolysis of the material in water leads to colloidal suspensions of nanosheets with lateral dimensions of about 20 nm and thicknesses of *ca*. 4 nm as demonstrated by atomic force microscopy and dynamic light scattering. Atomic resolution scanning transmission electron microscopy combined with electron energy-loss spectroscopy confirm the high crystalline quality of the crystals and the proper Co/Fe stoichiometry. The magnetic properties of the CoFe-LDH have been investigated by means of DC and AC magnetic susceptibility measurements and isothermal magnetisation, showing a low-temperature magnetic ordering below *ca*. 7 K with a spin-glass like behaviour, and displaying hysteresis cycles at 2 K with a coercive field of 402 G. Moreover, the sample has been tested as electrode material for supercapacitors in a three-electrode system by means of cyclic voltammetry and galvanostatic charge-discharge experiments, showing high capacitances and stability. Finally, we have explored the electrocatalytic behaviour towards water oxidation, demonstrating its efficient and persistent performance under basic pHs, highlighting their tremendous potential in energy storage devices.

1. Introduction

Two-dimensional (2D) materials have attracted increasing interest in the last years due to their unique morphology and properties and their use for a variety of applications, ranging from electronics to gas storage or separation, catalysis, high performance sensors or inert protective coatings, among others.[1] Beyond graphene (G)[2], layered chalcogenides[3], phosphates[4], titanates[5], perovskites[6] and metal oxides or hydroxides[7] appear as promising alternatives to this ubiquitous 2D material, displaying complementary physical properties, that open the door for the development of new hybrid multifunctional materials.[8–10]

Layered double hydroxides (LDHs) are a family of inorganic 2D layered materials that have attracted increasing attention because of their interest in catalysis, adsorption, drug delivery, sensors, magnetism or energy storage.[11,12] These lamellar compounds can be described by the general formula $[M^{II}_{1-x}M^{III}_{x}(OH)_2]^{x+}(X^{n-})_{x/m}\ nH_2O$ in which M^{II} and M^{III} are divalent and trivalent metals (M^{II}=Mg, Zn, Ni, Co etc. and M^{III}=Al, Fe, Cr, Mn etc.) and X^{n-} is the interlayer anion (typically carbonate, nitrate, chloride etc.) compensating the positive charge of the layers.

The conventional methods for synthesizing LDH-based materials are the coprecipitation at variable or constant pH, and the most recently procedures based on ammonia releasing reagents (ARR), which enable the synthesis of highly crystalline micrometric-sized particles. All these synthetic routes were developed in aqueous solution, leading to LDHs with strong interlayer electrostatic interactions, which can hardly be exfoliated under mild conditions. Thus, organic polar solvents like formamide are often required to obtain unilamellar nanosheets.[13] The obtention of positively charged monolayers (*ca*. 0.8 nm in thickness) of LDHs is a topic of utmost importance, as this nanometric entities can be employed as extremely useful building blocks in the design of novel heterostructured materials.[7,1,13]

Gardner *et al.* have reported aqueous transparent colloidal suspensions of LDH particles that exhibit increased surface-to-surface interactions.[14,15] This procedure consists on the non-aqueous synthesis of Al-containing alkoxide-intercalated LDHs that undergo complete hydrolysis in water obtaining colloidal solutions. This synthetic procedure leads to crystals with sizes below 100 nm, in sharp contrast with the micrometric crystals obtained by ARR methodologies. The nanometric sizes exhibited by these alkoxide-intercalated LDHs could have a significant influence on the magnetic behaviour or electrochemical properties of LDHs, due to some size-dependent magnetic phenomena or an increase in the specific surface area, respectively. This innovative synthetic route has been scarcely employed to date.[13] Indeed, the only reported examples are the NiMn-LDHs, successfully used in the development of high capacity hybrid Li-ion batteries[16], and more recently, hybrid NiCo-LDHs[17] and Co- or Mn- containing LDHs,[18] which have been tested as electrode materials for supercapacitors, exhibiting high specific capacity. Remarkably, to the best of our knowledge, no magnetic studies have been performed for these alkoxide-containing LDH materials.

Herein, we have synthesized and thoroughly characterized (*via* scanning transmission electron microscopy (STEM) techniques, atomic force microscopy (AFM) and magnetic measurements) alkoxide-intercalated CoFe-LDHs of *ca*. 20 nm in size, these materials exhibit low-temperature magnetism. More interestingly their electrochemical behaviour makes them useful as electrode materials for supercapacitors and as Oxygen Evolution Reaction (OER) electrocatalysts.

2. Experimental section

2.1 Chemicals

Poly(vinylidene fluoride), $(CH_2CF_2)_n$ (PVDF, Sigma Aldrich); Carbon black, acetylene 50%

compressed (Alfa Aesar, 99.9%); $CoCl_2.6H_2O$, $FeCl_3.6H_2O$ (Sigma-Aldrich); Lithium Perchlorate, $LiClO_4$ (Aldrich); Sodium Nitrate, $NaNO_3$ (Merck); Potassium Hydroxide, KOH (Panreac, 99%); Methanol (Panreac 99.9%); Ethanol (Panreac,98%) and Acetonitrile (Panreac 99.9%) were used as received, ultrapure water was obtained from a Millipore Milli-Q equipment.

2.2 Synthesis of CoFe-LDH:

Synthesized following a modified method described by Gardner et al.[14,15]

In a typical procedure, chloride salts of the metals with a stoichiometry ratio of 3:1, $CoCl_2.6H_2O$ (30 mM, 714 mg) and $FeCl_3.6H_2O$ (10 mM, 270 mg), were added into a three-neck flask and then dissolved with 100 mL of methanol, reaching a total metal cation concentration of 40 mM. The solution was then stirred and heated at 65 ºC during 1 h. Afterwards, a solution containing 3.8 g of NaOH in 100 mL of MeOH was slowly added to the previous solution (the addition should last at around 2-3 minutes) and the mixture was left 72 h under stirring at 65 $^{\circ}$C. A constant pressure of Ar atmosphere was employed to avoid the carbonate contamination and the evaporation of the MeOH. Finally, the resultant brown fine powder product was filtered, washed with MeOH and dried in a vacuum.

$[Co_{0.75}Fe_{0.25}(OH)_{1.3}(OMe)_{0.7}](Cl)_{0.25} \cdot 0.6H_2O$; (C,H,N, calc: 7.1, 2.1, 0; found: 7.12, 2.34, 0.16).

2.3 Exfoliation of CoFe-LDH:

In order to exfoliate the CoFe-LDH platelets in water, typically 10 mg of the sample were dissolved in 10 mL of Milli-Q water and then the mixture was sonicated during 30 min. Afterwards, the solution was centrifuged at 2000 rpm 10 minutes and sonicated again for 30 min more. The colloidal suspension was then taken to carry out the measurements over the exfoliated platelets.

2.4 Synthesis of CoFe-LDH-Coprecipitation:

Synthesized following the method described by Rives et al.[19]

In a typical procedure, the nitrate salts of the metals 0.012 mol of $Co(NO_3)_2.6H_2O$ and 0.006 mol of $Fe(NO_3)_3.9H_2O$ were dissolved in 25 mL of mili-Q water (previously boiled in a microwave (MW) and stored under argon atmosphere during 1 hour) and then the solution was dropwise added (ca. 30 drops min^{-1}) to a solution containing 0.031 mol Na_2CO_3 in 50 ml of mili-Q water (previously boiled in a MW and stored under argon atmosphere during 1 hour). The resulting mixture was stirred at 70 ^oC for 30 h under argon atmosphere (with the system sealed hermetically). After that, the light brown fine powder was filtered, washed thoroughly with Milli-Q water and EtOH and dried in a vacuum. Further characterization can be found on SI1.

2.5 Physical characterization

Real space studies of the samples were carried out by aberration corrected scanning transmission electron microscopy (STEM) and electron energy-loss spectroscopy (EELS) in a JEOL JEM-ARM200CF electron microscope equipped with a spherical aberration corrector and a Gatan Quantum EEL spectrometer, operated at 200 kV. Samples were prepared by dropping a colloidal suspension of the fresh sample in Milli-Q water on a holey carbon-coated copper grid for STEM-EELS observation. Field emission scanning electron microscopy (FESEM) studies were performed on a Hitachi S-4800 microscope operating at an accelerating voltage of 20 kV and without metallization of the samples. Thermogravimetric analysis (TGA) of all compounds were carried out with a Mettler Toledo TGA/SDTA 851 apparatus in the 25–800 °C temperature range under a 10 °C min^{-1} scan rate and an air flow of 30 mL min^{-1}. X-ray diffraction (XRD) patterns were obtained using a Philips X'Pert

diffractometer using the copper radiation (Cu-Kα = 1.54178 Å). Infrared spectra were recorded in a FT-IR Nicolet 5700 spectrometer in the 4000–400 cm^{-1} range with a nominal resolution of 0.4 cm^{-1}. Atomic force microscopy (AFM) measurements were collected in a Multimode atomic force microscope (Veeco Instruments, Inc.). Typically, a freshly diluted emulsion resulting from the hydrolysis of CoFe−LDH samples in water was deposited onto a clean Si wafer by spin coating at 5000 rpm. The images were obtained with a Si tip (frequency and K of ≈300 kHz and 42 $N \cdot m^{-1}$, respectively) using the tapping-mode in air at room temperature. Images were recorded with 512 X 512 pixel and a 0.5−1 Hz scan rate. Processing and analysis of the images were carried out using the Nanotec WSXM-4.0 Beta 6.5 software (www.nanotec.es).[20] Dynamic light scattering (DLS) measurements were recorded at 25 ^{o}C with a Zetasizer Nano ZS instrument (Malvern Instrument Ltd.) on a freshly exfoliated sample as described before. Magnetic measurements were carried out with a Quantum Design superconducting quantum interference device (SQUID) MPMS-XL-5. The susceptibility data were corrected from the diamagnetic contributions of the atomic constituents of the samples as deduced from Pascal's constant tables and the sample holder. The dc data were collected under an external applied field of 100 or 1000 G in the 2–300 K temperature range. Magnetization studies were performed between −5 and +5 T at a constant temperature of 2 K.

2.6 Electrochemical measurements

The electrochemical experiences were executed using an Autolab electrochemical workstation (PGSTAT-100 potentiostat/galvanostat) connected to a personal computer that uses GPES electrochemical software.

The materials were mixed with acetylene black and PVDF in a mass ratio of 80:10:10 in

ethanol and deposited in a nickel foam electrode. The as-prepared nickel foam electrodes were dried overnight at 70 ºC and pressed. Each working electrode contained about 1 mg of electroactive material and had a geometric surface area of about 1 cm^2. A typical three-electrode experimental cell equipped with a stainless steel plate having 4 cm^2 of surface area as the counter electrode, and a Metrohm Ag/AgCl (3 M KCl) as the reference electrode was used for the electrochemical characterization of the nanocomposite materials trapped by the working electrodes.

The electrochemical measurements were carried out in KOH aqueous solutions as the electrolyte at the indicated concentrations. Ultrapure water was obtained from Milli-Q equipment. The specific capacitance (C), was calculated from the cyclic chronopotentiometric curves according to Equation (1):

$C = I\Delta t/m\Delta V$ (1)

where I is the charge/discharge current, Δt is the time for a full charge or discharge, m the weight in grams of the active material in the electrode layer, and ΔV is the voltage change after a full charge or discharge.

The electrocatalytic properties were studied in the aforementioned working electrodes, measuring the CV at a scan rate of 5 mV/s in 0.1 M and 1 M KOH aqueous solutions. In addition, chronoamperometric studies were performed at constant potentials (0.83 V for 0.1 M KOH, and 0.75 V for 1 M KOH). All potentials reported in this manuscript were converted to the NHE reference scale using E(NHE) = Eº(Ag/AgCl) + 0.197 V.

3. Results and discussion

The synthesis of the CoFe-LDH was performed in non-aqueous media by following a modified synthetic method reported by Gardner et al.[14] In this synthesis, a methanolic solution

including the metal chloride salts was mixed with a NaOH solution at 65 ºC. After 72 h a brown precipitate was obtained, then the particles were filtered and washed thoroughly with methanol. The dark-brown powder was then placed in a vacuum chamber in order to avoid the carbonate contamination. On the basis of microanalysis, thermogravimetric and elemental analysis, the proposed chemical formula was estimated to be: $[Co_{0.75}Fe_{0.25}(OH)_{1.3}(OMe)_{0.7}](Cl)_{0.25} \cdot 0.6H_2O$; Co/Fe = 3 : 1.

The formation of the LDH phase was confirmed by Powder X-ray diffraction (PXRD), exhibiting the typical hydrotalcite-like profile with (00*l*) basal reflections at low angles and the characteristic (110) doublet at around 60º in 2θ. The estimated basal space is of 9.21 Å, in excellent accordance with that reported for an MgAl-Cl-MeOH LDH.[14] The broadness of the peaks indicates that the sample is composed by nanometric particles, in clear contrast with expected for a traditional coprecipitated LDHs. In this sense, for comparative purposes Fig. 1 shows the PXRD pattern of a sample synthesized by means of the traditional coprecipitation approach (CoFe-LDH Cop).[19] In this case, well-defined sharp peaks could be observed, with a basal space of 7.59 Å indicating the sole presence of carbonate as interlamellar anion (SI1).[19]

Fourier transform infrared (FT-IR) spectroscopy was also used for study the nature of the intercalated moieties. In addition to the characteristic M-O bands related to the brucite-like structure at low frequencies, significant bands appeared at around 2926 and 1070 cm^{-1}, indicative of C-H bonds and C-O bonds, respectively, confirming the presence of methoxide in the interlamellar space of the CoFe hydroxide layers (Fig.1B). Moreover, the broad band centred at *ca*. 3416 cm^{-1} is related with the combination of the stretching vibration of the hydroxide groups in the layers and the interlayer water molecules (ν_{OH}). Interestingly, if the sample is stored in the presence of air for several days, a band corresponding to CO_3^{2-}

absorption appeared at around 1448 cm^{-1} (C=O asymmetric stretching vibration), as previously reported for several LDH-based hybrids by Iyi and co-workers, demonstrating the high CO_2 affinity of these alkoxide-intercalated LDHs (See Fig.1B).[21]

Thermogravimmetric analysis (Fig.1C) was also performed in air showing an initial loss (*ca.* 10 wt.%) of physisorbed water molecules at low temperatures. As the temperature is increased to 300 ºC, an abrupt mass loss (*ca.* 14 wt.%) corresponding to the elimination of interlamellar chemisorbed water, followed by decomposition of the organic moiety and the dehydroxilation of the layers takes place (300-500ºC), accounting for a weight loss of about 34% in total.[21]

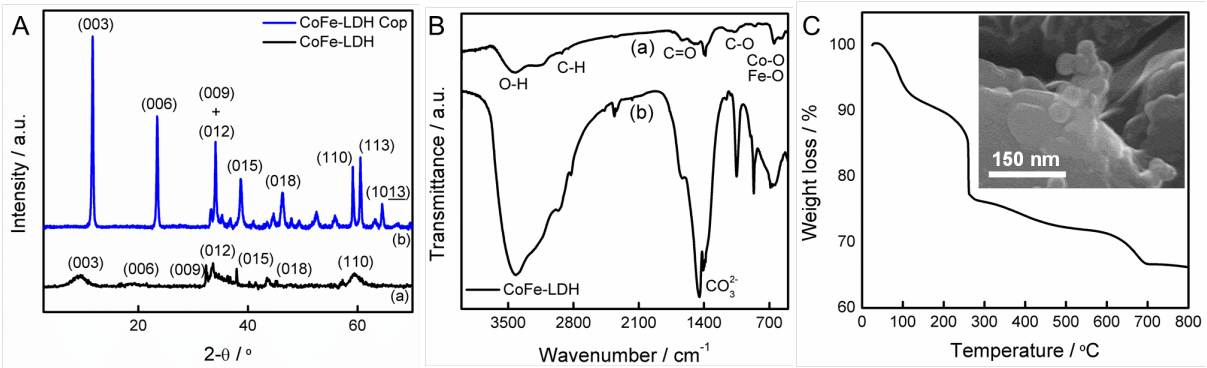

Figure 1. (A) XRD patterns of nanosized alkoxyde intercalated **CoFe-LDH** (a) and carbonate intercalated **CoFe-LDH Cop** synthesized *via* conventional coprecipitation route (b), showing the characteristic reflections of the LDH phase. (B) FT-IR spectra of freshly prepared CoFe-LDH (a) and the powder stored open to the ambient air (b), highlighting the carbonate incorporation into the LDH. (C) Thermogravimetric analysis of CoFe-LDH. The inset represents a FESEM image of CoFe-LDH nanoplates.

The morphology of the CoFe-LDHs was examined by FESEM. Inset in Fig.1C, shows homogeneous samples displaying weak contrast consisting on small platelet-like particles

with nanometric lateral dimensions. The nanoparticles seems to be well oriented in a plane-to-plane disposition, in clear contrast with that expected for a higher aspect ratio relation samples of several hundreds of nanometers in size, accordingly to that reported for MgAl-LDHs by Gardner[15] or Hibino[22] and co-workers. The Fe/Co atomic ratio was confirmed by means of EDAX microanalysis, showing an experimental value of 0.34, in excellent accordance with the nominal composition. Thus, in the series of FESEM images of the CoFe-LDH sample, a homogeneous distribution of Co and Fe atoms at the nanometric scale can be seen (Fig. SI 2).

To gain further insight on the microstructure of the nanoparticles, we analyzed the sample by aberration-corrected STEM-EELS. Fig. 2A shows a low magnification high angle annular dark field (HAADF) STEM image of the particles. The platelet-like nanocrystals have an average lateral size of 12-18 nm. Fig. 2B shows an EELS spectrum obtained while illuminating a crystal while scanning the electron beam in order to minimize beam induced damage. The O *K* edge, Fe $L_{2,3}$ edge and Co $L_{2,3}$ edges are visible, near 530 eV, 709 eV and 779 eV, respectively. The quantification of the spectrum using the routine available in the Gatan Digital Micrograph software (and Hartree-Slater cross-sections) yields a Fe/Co atomic ratio of 0.31±0.04, in good agreement with EDAX microanalysis. High magnification atomic resolution images show a high quality crystalline structure (Fig. 2C). Some stacking faults are observed along with occasional lacks of periodicity in the atomic chains, probably related with some disruptions in the cation ordering of the samples.[23,24]

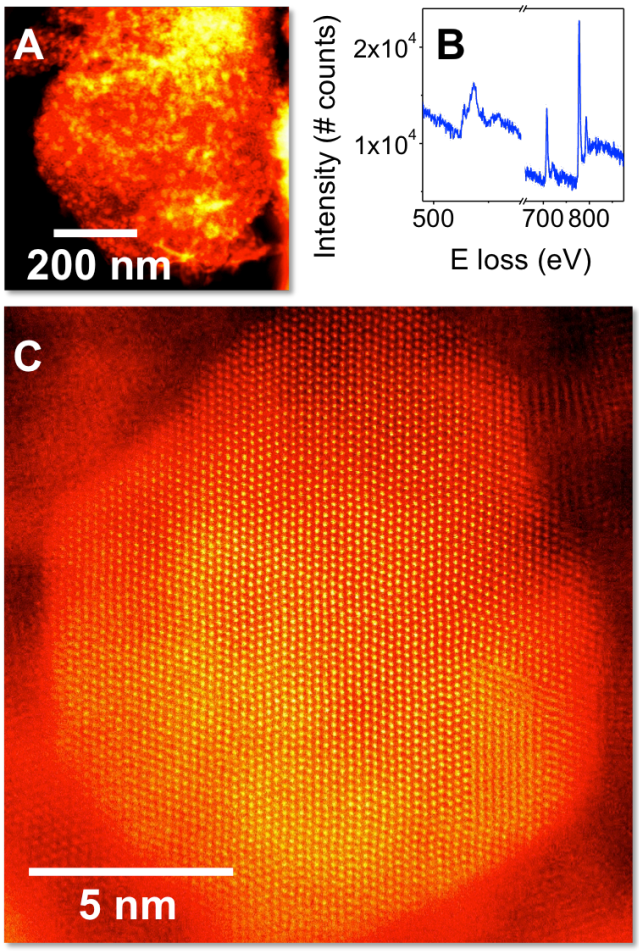

Figure 2. (a) Low magnification HAADF image. (b) EEL spectrum showing the O *K* edge, Fe $L_{2,3}$ edge and Co $L_{2,3}$ edges. (c) Atomic resolution HAADF image of a 2D platelet crystal, obtained at 200 kV.

At this point, it is well known the ability of other alkoxyde intercalated LDHs to serve as precursors of colloidal nanosheet suspensions after their aqueous hydrolysis.[14–16] In this sense, we have explored the hydrolysis of our sample suspending *ca*. 10 mg of CoFe-LDH in 10 ml of Milli-Q water. The suspension was successively sonicated and centrifuged before characterizing the resulting colloidal suspension. After initial sonication, the Tyndall effect (indicative of the light scattering of nanometric particles) can be clearly observed, showing a translucent colloidal solution of brown color, as previously reported by Sasaki and co-workers

for micrometric $Co^{2+}Fe^{3+}$-LDHs exfoliated in formamide (Fig. 3).[25] Direct information of the size of the colloidal suspension in water was obtained from Dynamic Light Scattering (DLS) experiments (Fig. 3A). We observe that the average hydrodynamic diameter, that is a complex function of both the diameter and the particle size for anisotropic materials like LDHs, describes a Gaussian distribution of the size of the particles centred on *ca*. 26 nm in excellent agreement with the electron microscopy observations. In addition, we always observe a less intense peak of particle aggregates at about 530 nm.

Furthermore, we have investigated the particle size and thickness by means of tapping mode AFM taking advantage of the topological precision of this technique. We have decorated a SiO_2 substrate by spin-coating with our colloidal aqueous suspension, and afterwards we have studied their morphology. Fig. 3B exhibits a 3D AFM image of 550 nm x 550 nm area showing well-dispersed single particles. The cross-sectional analysis corresponding to the highlighted areas **1** and **2** in the topography image shows small nanoparticles with a thickness of about 4 nm and smooth rounded shapes of *ca*. 37, 18 and 13 nm, respectively (Fig. 3C and D). From the analysis of several exfoliated crystals we have measured an average particle size and height of 25,7 ± 8,6 nm and 4,6 ± 0,8 nm, respectively (See SI 3). Therefore, we can consider the exfoliated particles as a few-layers CoFe-LDHs. With the lateral dimensions extracted from electron microscopy and the thickness observed in AFM studies corresponding to 5-8 monolayers, we can estimate an aspect ratio relation of 4, that is even smaller than that observed for submicrometric MgAl-LDH nanoplatelets suspended in water as reported by Xu et al.[26,27]

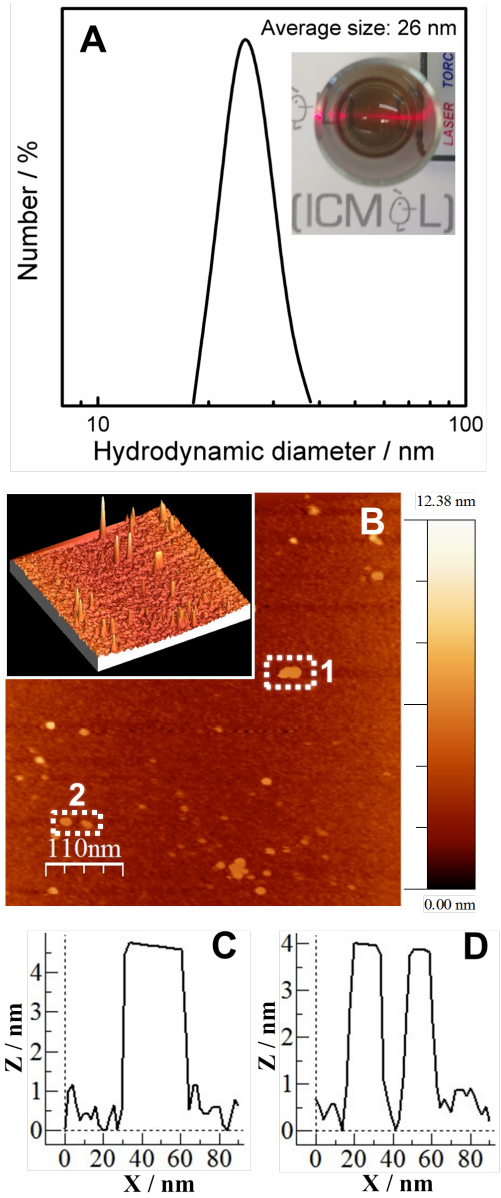

Figure 3. (A) Distribution of sizes as extracted from DLS measurements for the CoFe-LDH. The inset shows the clearly visible Tyndall effect, resulting from the scattering of the irradiated beam by the particles in solution, confirming the presence of exfoliated LDH nanosheets. (B) AFM topography image of the hydrolysed CoFe-LDH nanosheets deposited on a silicon wafer substrate by spin coating. The inset represents the corresponding three-dimensional image. (C) and (D) height profiles of the selected areas *1* and *2*, respectively.

As previously reported for several magnetic LDHs, CoFe-LDHs are expected to behave as ferrimagnets due to the coexistence of ferromagnetic Co-OH-Co superexchange interactions and antiferromagnetic Co-OH-Fe or Fe-OH-Fe interactions mediated by the -OH bridges.[28,29,24] Static magnetic measurements were performed in a superconducting quantum interference device (SQUID) with freshly prepared powdered samples. DC susceptibility exhibits an abrupt step jump at around 50 K indicative of cooperative magnetic interactions (Fig. 4A). The corresponding thermal variation of the product of the molar magnetic susceptibility times the temperature ($\chi_M T$) decreases regularly from 2.48 emuKmol^{-1} at 300 K to a minimum of 1.98 emuKmol^{-1} at 55 K. Afterwards, the $\chi_M T$ product exhibits a sharp increase upon cooling reaching a maximum value of 5.55 emuKmol^{-1} at 6.7 K, and then sharply decreases to a value of 2.0 emuKmol^{-1} at 2 K (Table 1 and inset in Fig. 4A). The fitting of the dc data to the Curie-Weiss law above 50 K yield a negative value of the Weiss constant (θ) of -14.7 K indicative of strong AF interactions within the layers, and a Curie constant value (C) of 2.57 emuKmol^{-1} in good agreement with that expected for a magnetically diluted combination of Co^{2+} (S = 3/2) and Fe^{3+} (S = 5/2) ions in the ratio previously determined by electron probe microanalysis (Inset in Fig. 4A). Field cool (FC) and zero-field cooled (ZFC) experiments indicated the presence of cooperative magnetism, presenting a clear bifurcation below an irreversible temperature (T_{irr} = 4.8 K) and a ZFC broad maximum at *ca*. 4.4 K (Fig. 4B).

Table 1. Main magnetic data and parameters for CoFe-LDH.[a]

χT_{rt} (emu·K·mol^{-1})	C_{SO} (emu·K·mol^{-1})	C (emu·K·mol^{-1})	Θ (K)	T_{irr} (K)	T_B (K)	T_M (K)	M_S (50 kG) (μ_B)	M_R (μ_B)	H_{Coer} (G)	Δ/k_B (K)	ν_0 (Hz)	ϕ
2.48	2.50	2.57	-14.69	4.8	4.4	7.0	0.98	0.07	402	116.9	3.8X10^{14}	0.063

[a] χT value at room temperature [χT_{rt}, (emu·K·mol^{-1})], expected spin-only value of the Curie constant [C_{so}, (emu·K·mol^{-1})], experimental Curie constant [C, (emu·K·mol^{-1})], Weiss constant (Θ), temperature of the divergence of the ZFC and FC magnetic susceptibility (T_{irr}), blocking temperature extracted from ZFC curve (T_B), temperature for the onset of spontaneous magnetization extracted from χ″ plot (T_M), saturation magnetization (M_S), remnant magnetization (M_R), coercive field at 2 K (H_{Coer}). Energy barrier (E_a/k_B) and frequency factor (ν_0), resulting from the fitting of the magnetic susceptibility to the Arrhenius law. Mydosh parameter (ϕ). $S(Co^{2+}) = 3/2$, $S(Fe^{3+}) = 5/2$.

The long-range magnetism was further confirmed by *ac* dynamic measurements, showing the onset of spontaneous magnetization (T_M) at *ca*. 7.0 K (Fig. 4C). This value is smaller than that exhibited by NiFe-LDH and NiCr-LDH synthesized by ARRs methodologies (16.5-16.8 K and 19.5-21 K, respectively) and is indicative of size effects.[24,30] Otherwise, the CoFe-LDH T_M value is slightly higher than those reported for any NiAl- or CoAl-LDHs (< 7 K), independently of the particle size and the synthetic methodology used, indicative of a higher extent of F and AF magnetic interactions.[31,28,26,32] Moreover, both the in-phase and out-of-phase signals of the *ac* data exhibit frequency dependence. The frequency dependence of the χ''_M maxima was quantified with the frequency-shift parameter introduced by Mydosh.[33] Thus, this peak shows a frequency dependence whose normalized variation, measured as the peak shift per decade of frequency, $\Delta T_{max}/T_{max}\Delta(Log\ \nu)$, is 0.058-0.063 (depending on the T_{max} value used). It is worth mentioning that this value is much larger than the typical values observed in canonical spin glasses (0.005-0.018) and is similar to that observed for spin-glass like materials (0.06-0.08) such as nanosized NiAl- and CoAl-LDHs[31], $CoAl(OH)_6(DDS)_x$–LDHs nanoplatelets[26] and NiFe-CoTPPS hybrids[34]. Furthermore, the fitting of the frequency dependence of χ''_M to an Arrhenius law yields a value for the energy barrier of Δ/k_B=116.9 K, which is consistent with that of a superparamagnet.[33] This activated behaviour in the CoFe-

LDH nanoparticles is probably related with a superparamagnetic size effect,[26,35] in addition to the spin-glass like nature intrinsic to LDHs,[24] indicating that the nanometric dimensions play a crucial role on the magnetic properties of the LDHs. In this sense, the magnetic behaviour of the CoFe-LDH Cop sample whose average size is of several hundred nanometers (See SI 1.IV) was also measured, showing the presence of extrinsic impurities and a higher T_M value of *ca*. 11 K (See SI 4 for further details). Moreover, Fig. 4D exhibits the field-dependent magnetization at 2K under an applied field up to 5 T, showing a small coercive field of *ca*. 402 G, which indicates the soft magnetic character of this nanomaterial.

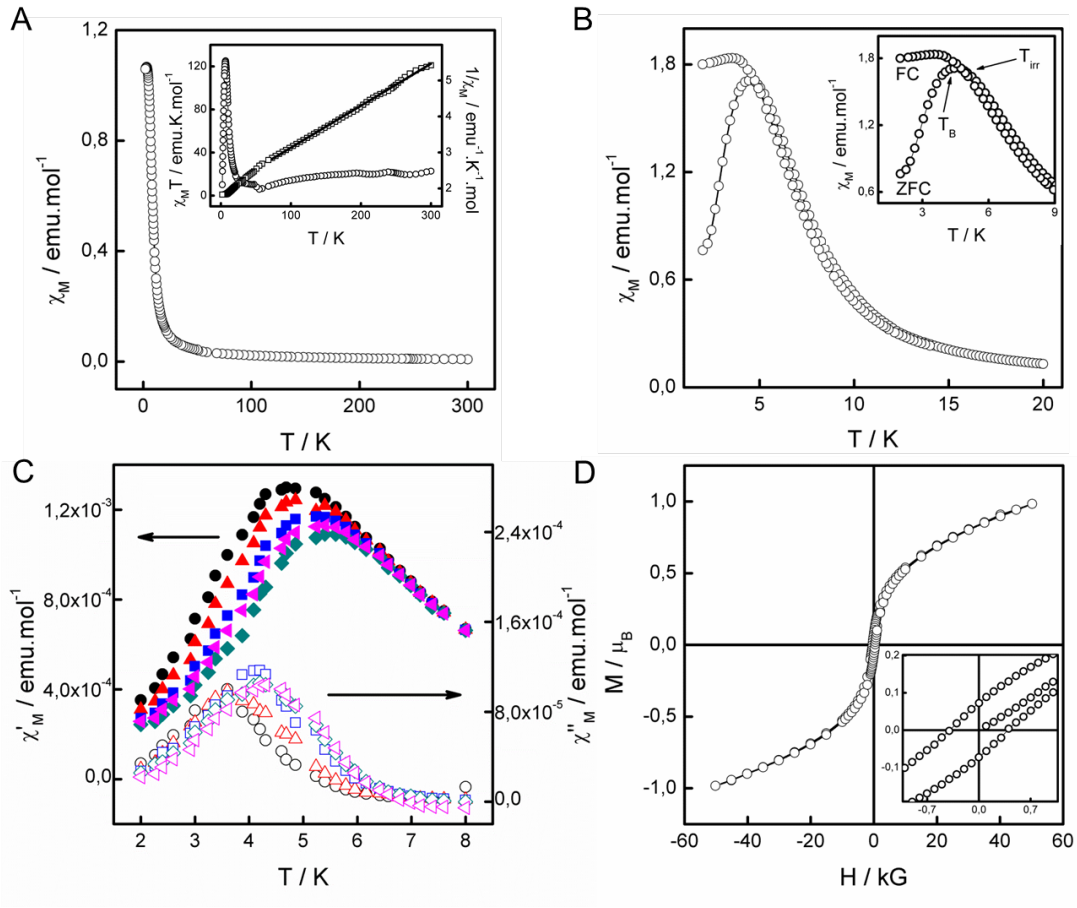

Figure 4. Magnetic properties of CoFe-LDH. (A) χ_M *vs* T plot. The inset represents the temperature dependence of the χ_M T product and the fitting (solid line) of the magnetic susceptibility data to a Curie–Weiss law. (B) ZFC-FC molar magnetization. The inset

highlights the low temperature region showing the bifurcation point (T_{irr}) and the blocking temperature (T_B). (C) Thermal dependence of the in-phase (χ'_M) and out-of-phase (χ''_M) signals at different frequencies from 1 to 997 Hz. (D) Hysteresis cycle at 2 K. The inset shows the low field region.

One of the most relevant aspects of LDHs is their applicability in energy storage devices like Li-ion batteries, supercapacitors (SCs) or water splitting devices.[36] In this context, SCs represent an avenue worth exploring due to the potential to deliver high power densities under short periods of time with high cyclability and durability.[37] SCs are mainly utilized for industrial stationary applications, automotive transportation and portable electronic applications.[38]

We have tested the CoFe-LDH sample as electrode material for SCs in a conventional three-electrode cell. The CoFe-LDH powdered sample was mixed with acetylene black and polyvinilidene fluoride in a mass ration of 80:10:10 with etanol.[39] The resulting slurry was casted on a 1cm^2 Ni-foam, dried and pressed to minimize the loose of the active material during the electrochemical testing. The electrochemical properties were measured by means of cyclic voltammetry (CV) using 6 M KOH as electrolyte under an applied voltage range of -0.4-0.4 V (vs. Ag/AgCl). CV in Fig. 5A reveals a pseudocapacitive behaviour with peaks related to the oxidation of Co (e.g. from Co^{2+} to Co^{3+} and then to Co^{4+}) while cathodic peaks indicate the reduction of Co (e.g. Co^{4+} to Co^{3+} and then to Co^{2+}). In addition, the effect of the scan rate was also studied, Fig. SI 5 shows that the cathodic and anodic peak currents (i_p) exhibit an almost linear relationship with the square root of the scan rate ($\nu^{1/2}$), indicating a diffusion-controlled process, in which the electrolyte plays an important role in the pseudocapacitance.[40] All these results support the use of these nanoparticles as electrode material for supercapacitive devices.[18]

Galvanostatic charge-discharge cycling was also measured in order to study the specific capacitance of this material (Fig. 5B). A large discharge capacity of *ca*. 145 Fg^{-1} was obtained for a current density of 1 Ag^{-1} (Fig. 5C), overpassing that recently reported (138 Fg^{-1} at 20 mAg^{-1}) for a similar CoFe-LDH phase.[18] Moreover, a comparison with other recently reported Co-containing LDH materials reveals that CoFe-LDH presents good specific capacity values if compared with CoNiAl-LDH (90 Fg^{-1} at 1 Ag^{-1}) or Co_2Al-LDH (190 Fg^{-1} at 1 Ag^{-1}) synthesized by the traditional coprecipitation method.[41] The CoFe-LDH exhibits a multi-site pseudo-capacitive behaviour similar to that reported by Mousty and co-workers for CoAl-LDHs,[36,41] and is quite similar to that reported for novel layered parallel folding Co_3O_4 nanostructures, in which the formation of superficial cobalt oxyhydroxide (CoOOH) plays a crucial role in the pseudocapacitive behaviour, yielding values close to 200 Fg^{-1} at 1Ag^{-1}.[42] The capacity retention was also studied for the first 100 cycles, obtaining excellent values with no apparently loss of capacity after the first 100 cycles as depicted in Fig. 5D. It is worth noting that large measuring periods lead to partial loss of the active material. Interestingly, the CoFe-LDH Cop sample exhibits an excellent behaviour as electrode material for supercapacitors with remarkably higher values of specific capacitance, *e.g*. 505 Fg^{-1} at 2 Ag^{-1}. This enhanced performance is probably related with the presence of active extrinsic impurities, different particle size, porosity and/or crystallinity. Works in progress are trying to clarify these aspects. (See further details on SI 6).

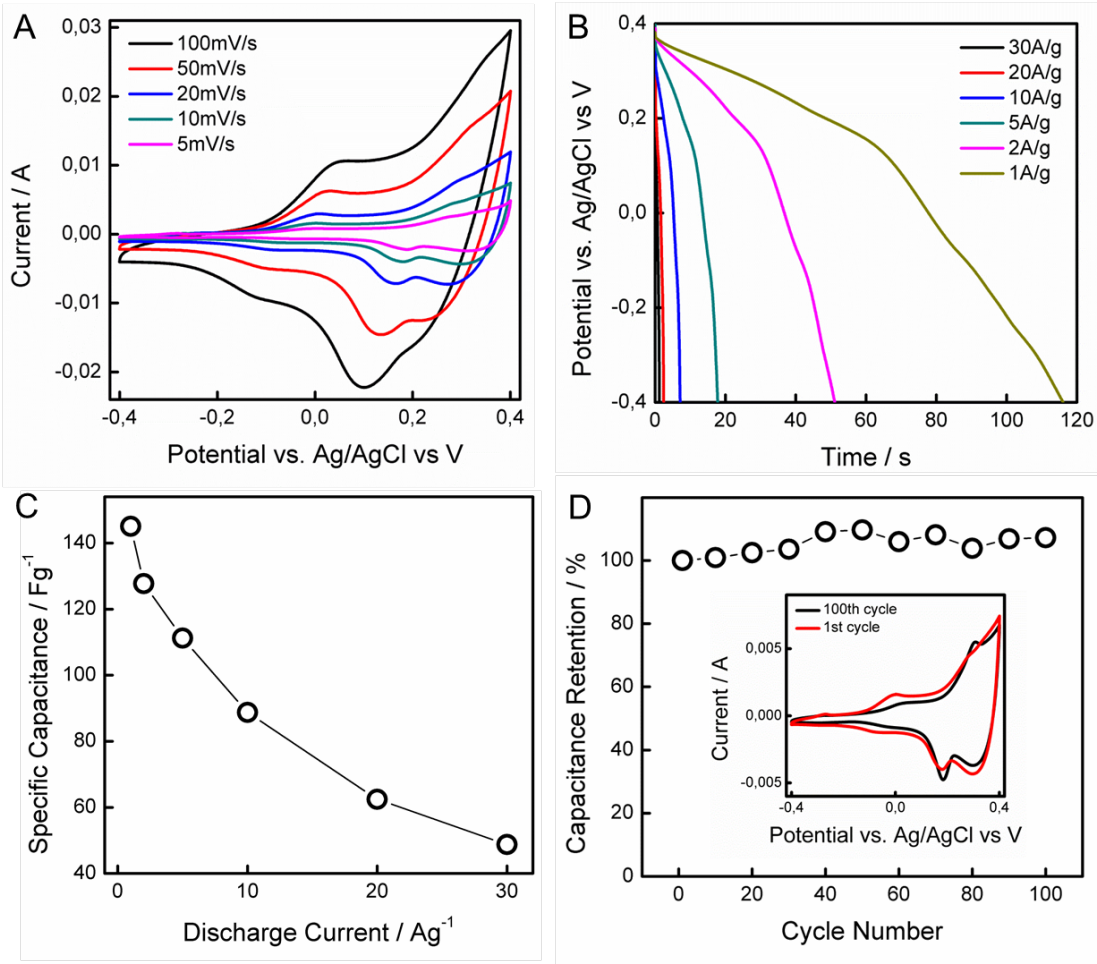

Figure 5. Electrochemical properties of CoFe-LDH. (A) CV curves at various scan rates in 6 M KOH aqueous solution. (B) Galvanostatic discharge curves and (C) specific capacitance of the material at different discharge current densities. (D) Specific capacitance vs. cycle number at a current density of 10 Ag^{-1}. The inset represents the CV curves corresponding to the 1st and the 100th cycle at 10 mVs^{-1}.

Finally, it is believed that the inclusion of active metals like Co or Fe in the LDH layers could promote the electrocatalytic behaviour of these moieties towards the oxygen evolution reaction (OER).[43,44] In fact, preliminary data indicated that the CoFe-LDH nanosheets evolve oxygen under an applied anodic potential. Along this front, we have explored the linear sweep voltammetry (LSV) curves at basic pH (0.1 M and 1 M KOH) under a slow scan rate of 5

mVs^{-1} in order to avoid diffusion limitations and minimize the capacitive currents, showing the onset of the oxygen evolution around 0.60 V (pH=13; 0.797 V *vs* NHE) and 0.51 V (pH=14; 0.710 V *vs* NHE), which represents a required overpotentials of *ca*. 397 mV and 310 mV for hydroxide oxidation at 0.1 and 1 M KOH, respectively (Fig. 6A):

$$4OH^- \leftrightarrow O_2 + 2H_2O + 4e^-; \quad E^0 = 0.40 \text{ V}$$

The catalytic activity towards water oxidation at 1.0 V yields current densities (that is a measure of the catalytic activity) of 12.43 and 62.69 mAcm^{-2}, respectively. These values are higher than those reported for ZnCo-LDHs[43] (11.6 mAcm^{-2}, pH=13) or CoNi-LDHs[45] (1 mAcm^{-2} at 1.4 V_{NHE}, pH=7), and surpass that exhibited by Co_3O_4[43] (2.90 mAcm^{-2}, pH=13) as recently reported by Asefa and co-workers. LSV measurements of the CoFe-LDH Cop sample have been also performed, exhibiting a similar behaviour as depicted in SI 7. The onset of the oxygen evolution appears at around 0.57 V (pH=13; 0.767 V *vs* NHE) and 0.50 V (pH=14; 0.697 V *vs* NHE), respectively. Besides, the values of the current densities at 1.0 V are 8.86 mAcm^{-2} (pH=13) and 74.36 mAcm^{-2} (pH=14). In addition, Fig. 6B depicts the chronoamperometric curve of the CoFe-LDH-catalysed water oxidation reaction over 10000 s at 0.83 V at pH=13 and 0.75 V at pH=14, showing current densities higher than 3 and 10 mAcm^{-2}, respectively. The current-time plot reveals the persistence of the electrocatalytic activity under the studied timescale. This assumption was further confirmed by measuring the LSV after the long reaction period, that exhibits an almost similar profile, indicative of an excellent performance towards OER (See Fig. SI 8).

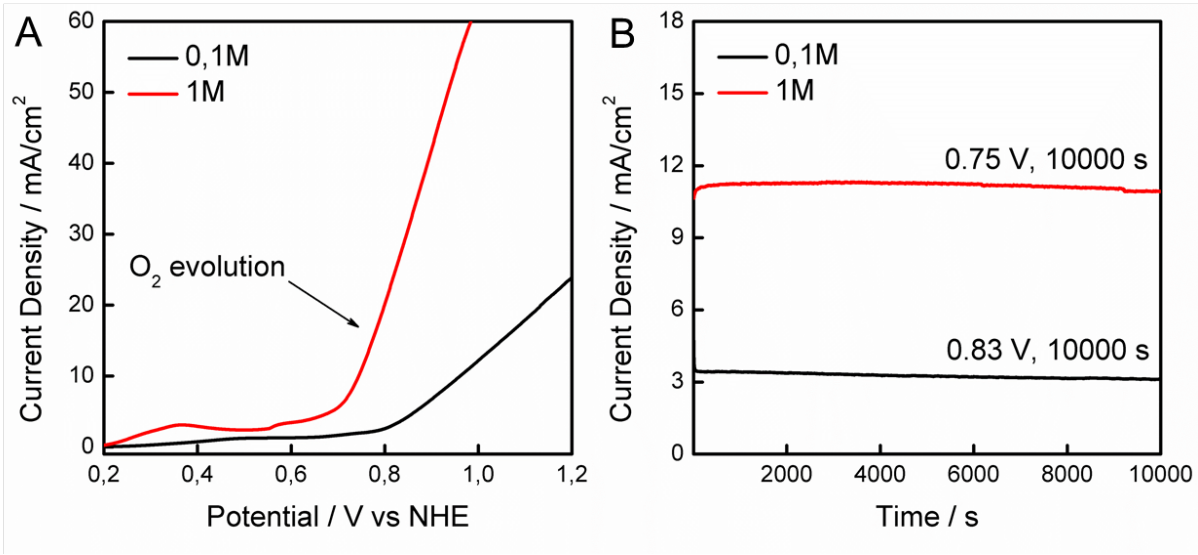

Figure 6. Electrochemical performance of CoFe-LDH OER electrocatalyst. (A) LSV curves in 0.1 M and 1 M KOH. (B) Current-time curve obtained for water oxidation reaction at 0.83 V (0.1 M) and 0.75 V (1 M) vs ENH.

The combination of Co and Fe in molecular-based materials for OER electrocatalysis has been recently reported for CoFe Prussian blues analogues, that in fact, exhibited very similar CV curves.[46] This preliminary result highlight the growing importance of LDHs as electrocatalytic materials as recently demonstrated for NiFe-LDH[44], CoNi-LDH[45], MnAl-LDH[47] or ZnCo-LDH[43]. Further work is still needed in order to improve the OER activity, optimizing the metal ratio composition and/or hybridizing these materials with conducting counterparts that could help to enhance the electron transport.[48,49]

4. Conclusions

In summary, we have shown how the use of a non-aqueous route for the synthesis of alkoxide-intercalated CoFe-LDH leads to crystalline anisotropic particles with a Fe:Co atomic

ratio of 1:3 that exhibit some structural disorder as revealed by STEM, and can be partially exfoliated in water through the hydrolysis of the alkoxide moieties. Our CoFe-LDHs nanosheets exhibit a superparamagnetic behaviour with a temperature for the onset of the spontaneous magnetization of *ca*. 7 K, with no signal of extrinsic magnetic impurities. Finally, electrochemical measurements have demonstrated its electrode functionality as supercapacitive material, exhibiting high specific capacitance values, and furthermore its excellent performance as OER electrocatalysts in basic media. Our results suggest that aqueous colloidal suspensions of CoFe-LDH nanosheets are good candidates for being used as building blocks in the development of more sophisticated hybrid nanostructures, for example hybridizing, with carbon nanostructures.[48] Moreover, these layered Co-containing systems can be envisaged as good electrode materials for supercapacitors, Li-ion batteries[13,16] or effective electrocatalyst towards the oxygen evolution reaction[44,36,50], underscoring a promising future to this earth-abundant nanostructured alkoxide-intercalated LDHs.

References

1. R. Mas-Ballesté, C. Gómez-Navarro, J. Gómez-Herrero, and F. Zamora, *Nanoscale*, 2011, **3**, 20–30.
2. A. K. Geim and K. S. Novoselov, *Nat. Mater.*, 2007, **6**, 183–191.
3. Q. H. Wang, K. Kalantar-Zadeh, A. Kis, J. N. Coleman, and M. S. Strano, *Nat. Nanotechnol.*, 2012, **7**, 699–712.
4. A. Clearfield, *Comments Inorg. Chem.*, 1990, **10**, 89–128.
5. T. Sasaki, M. Watanabe, H. Hashizume, H. Yamada, and H. Nakazawa, *J. Am. Chem. Soc.*, 1996, **118**, 8329–8335.
6. Y.-S. Han, I. Park, and J.-H. Choy, *J. Mater. Chem.*, 2001, **11**, 1277–1282.
7. R. Ma and T. Sasaki, *Adv. Mater.*, 2010, **22**, 5082–5104.
8. P. Gómez-Romero and C. Sanchez, *Functional Hybrid Materials*, John Wiley & Sons, 2006.
9. G. Rogez, C. Massobrio, P. Rabu, and M. Drillon, *Chem. Soc. Rev.*, 2011, **40**, 1031.
10. M. Clemente-León, E. Coronado, C. Martí-Gastaldo, and F. M. Romero, *Chem. Soc. Rev.*, 2011, **40**, 473.
11. V. Rives, *Layered Double Hydroxides: Present and Future*, Nova Publishers, 2001.
12. X. Duan and D. G. Evans, *Layered Double Hydroxides*, Springer, 2006.
13. Q. Wang and D. O'Hare, *Chem. Rev.*, 2012, **112**, 4124–4155.
14. E. Gardner, K. M. Huntoon, and T. J. Pinnavaia, *Adv. Mater.*, 2001, **13**, 1263–1266.
15. J. A. Gursky, S. D. Blough, C. Luna, C. Gomez, A. N. Luevano, and E. A. Gardner, *J. Am. Chem. Soc.*, 2006, **128**, 8376–8377.
16. M. Latorre-Sanchez, P. Atienzar, G. Abellán, M. Puche, V. Fornés, A. Ribera, and H. García, *Carbon*, 2012, **50**, 518–525.
17. H. Chen, L. Hu, M. Chen, Y. Yan, and L. Wu, *Adv. Funct. Mater.*, 2013, n/a–n/a.
18. Z. P. Xu, L. Li, C.-Y. Cheng, R. Ding, and C. Zhou, *Appl. Clay Sci.*, 2013, **74**, 102–108.
19. M. del Arco, R. Trujillano, and V. Rives, *J. Mater. Chem.*, 1998, **8**, 761–767.
20. I. Horcas, R. Fernández, J. M. Gómez-Rodríguez, J. Colchero, J. Gómez-Herrero, and A. M. Baro, *Rev. Sci. Instrum.*, 2007, **78**, 013705.
21. N. Iyi, Y. Ebina, and T. Sasaki, *Langmuir*, 2008, **24**, 5591–5598.
22. T. Hibino and M. Kobayashi, *J. Mater. Chem.*, 2005, **15**, 653.

23. S. Cadars, G. Layrac, C. Gérardin, M. Deschamps, J. R. Yates, D. Tichit, and D. Massiot, *Chem. Mater.*, 2011, **23**, 2821–2831.

24. G. Abellán, E. Coronado, C. Martí-Gastaldo, J. Waerenborgh, and A. Ribera, *Inorg. Chem.*, 2013, **52**, 10147–10157.

25. R. Ma, Z. Liu, K. Takada, N. Iyi, Y. Bando, and T. Sasaki, *J. Am. Chem. Soc.*, 2007, **129**, 5257–5263.

26. C. J. Wang, Y. A. Wu, R. M. J. Jacobs, J. H. Warner, G. R. Williams, and D. O'Hare, *Chem. Mater.*, 2011, **23**, 171–180.

27. Z. P. Xu, G. S. Stevenson, C.-Q. Lu, G. Q. (Max) Lu, P. F. Bartlett, and P. P. Gray, *J. Am. Chem. Soc.*, 2006, **128**, 36–37.

28. E. Coronado, J. R. Galán-Mascarós, C. Martí-Gastaldo, A. Ribera, E. Palacios, M. Castro, and R. Burriel, *Inorg. Chem.*, 2008, **47**, 9103–9110.

29. G. Abellán, J. A. Carrasco, and E. Coronado, *Inorg. Chem.*, 2013, **52**, 7828–7830.

30. J. J. Almansa, E. Coronado, C. Martí-Gastaldo, and A. Ribera, *Eur. J. Inorg. Chem.*, 2008, **2008**, 5642–5648.

31. J. Pérez-Ramírez, A. Ribera, F. Kapteijn, E. Coronado, and C. J. Gómez-García, *J. Mater. Chem.*, 2002, **12**, 2370–2375.

32. G. Abellán, F. Busolo, E. Coronado, C. Martí-Gastaldo, and A. Ribera, *J. Phys. Chem. C*, 2012, **116**, 15756–15764.

33. J. A. Mydosh, *Spin glasses: an experimental introduction*, Taylor & Francis, London; Washington, DC, 1993.

34. G. Abellán, E. Coronado, C. J. Gómez-García, C. Martí-Gastaldo, and A. Ribera, *Polyhedron*, 2013, **52**, 216–221.

35. J. D. Rall and M. S. Seehra, *J. Phys. Condens. Matter*, 2012, **24**, 076002.

36. C. Mousty and F. Leroux, *Recent Pat. Nanotechnol.*, 2012, **6**, 174–192.

37. G. Wang, L. Zhang, and J. Zhang, *Chem. Soc. Rev.*, 2012, **41**, 797–828.

38. X. Li and B. Wei, *Nano Energy*, 2013, **2**, 159–173.

39. G. Abellán, E. Coronado, C. Martí-Gastaldo, A. Ribera, and T. F. Otero, *Part. Part. Syst. Charact.*, 2013, **30**, 853–863.

40. E. Scavetta, B. Ballarin, M.Gazzano, and D. Tonelli, *Electrochimica Acta*, 2009, **54**, 1027–1033.

41. P. Vialat, F. Leroux, C. Taviot-Gueho, G. Villemure, and C. Mousty, *Electrochimica Acta*, 2013, **107**, 599–610.

42. D. Wang, Q. Wang, and T. Wang, *Inorg. Chem.*, 2011, **50**, 6482–6492.

43. X. Zou, A. Goswami, and T. Asefa, *J. Am. Chem. Soc.*, 2013, **135**, 17242–17245.

44. M. Gong, Y. Li, H. Wang, Y. Liang, J. Z. Wu, J. Zhou, J. Wang, T. Regier, F. Wei, and H. Dai, *J. Am. Chem. Soc.*, 2013, **135**, 8452–8455.

45. Y. Zhang, B. Cui, C. Zhao, H. Lin, and J. Li, *Phys. Chem. Chem. Phys.*, 2013, **15**, 7363–7369.

46. S. Pintado, S. Goberna-Ferrón, E. C. Escudero-Adán, and J. R. Galán-Mascarós, *J. Am. Chem. Soc.*, 2013, **135**, 13270–13273.

47. S. Werner, V. W. Lau, S. Hug, V. Duppel, H. Clausen-Schaumann, and B. V. Lotsch, *Langmuir*, 2013, **29**, 9199–9207.

48. M.-Q. Zhao, Q. Zhang, J.-Q. Huang, and F. Wei, *Adv. Funct. Mater.*, 2012, **22**, 675–694.

49. Y. Liang, Y. Li, H. Wang, and H. Dai, *J. Am. Chem. Soc.*, 2013, **135**, 2013–2036.

50. H. Wang and H. Dai, *Chem. Soc. Rev.*, 2013, **42**, 3088.

Acknowledgements

Financial support from the EU (Projects HINTS and ERC Advanced Grant SPINMOL), the Spanish MINECO (Projects Consolider-Ingenio in Molecular Nanoscience, MAT2011-22785, and CTQ-2011-26507), and the Generalitat Valenciana (Prometeo Program, ISIC-Nano and Gerónimo Forteza Program) is gratefully acknowledged. Support from VLC/CAMPUS and INNCIDE program through Vicerectorat d'lnvestigació i Política Científica of the University of Valencia is also acknowledge. We also acknowledge E. Tormos and A. López for his help with the experimental work, and J.M. Martínez and G. Agustí for magnetic measurements. This research was sponsored by the Office of Basic Energy Sciences, Division of Materials Sciences and Engineering, U.S. Department of Energy (M.V.). Electron microscopy at the Centro Nacional de Microscopia Electrónica (UCM) sponsored by the ERC Starting Investigator Award STEMOX#239739.